

Manipulation of $J_{\text{eff}} = \frac{3}{2}$ states by tuning the tetragonal distortion

Yakui Weng^{1,*} and Shuai Dong^{2,†}

¹*School of Science, Nanjing University of Posts and Telecommunications, Nanjing 210023, China*

²*School of Physics, Southeast University, Nanjing 211189, China*

 (Received 9 August 2021; revised 16 September 2021; accepted 21 October 2021; published 29 October 2021)

The spin-orbit entangled quantum states in $4d/5d$ compounds, e.g., the $J_{\text{eff}} = \frac{1}{2}$ and $J_{\text{eff}} = \frac{3}{2}$ states, have attracted great interests for their unique physical roles in unconventional superconductivity and topological states. Here, the key role of tetragonal distortion is clarified, which determines the ground states of $4d^1/5d^1$ systems to be the $J_{\text{eff}} = \frac{3}{2}$ one (e.g., K_2NbCl_6) or the $S = \frac{1}{2}$ one (e.g., Rb_2NbCl_6). By tuning the tetragonal distortion via epitaxial strain, the occupation weights of $d_{xy}/d_{yz}/d_{xz}$ orbitals can be subtly modulated, competing with the spin-orbit coupling. Consequently, quantum phase transitions between the $S = \frac{1}{2}$ state and the $J_{\text{eff}} = \frac{3}{2}$ state, as well as between different $J_{\text{eff}} = \frac{3}{2}$ states, can be achieved, resulting in significant changes of local magnetic moments. Our prediction points out a reliable route to engineer new functionality of J_{eff} states in these quantum materials.

DOI: [10.1103/PhysRevB.104.165150](https://doi.org/10.1103/PhysRevB.104.165150)

I. INTRODUCTION

Controlling electronic states in materials is one of the most important topics of condensed matter physics, which can lead to new functional devices. In strongly correlated electronic systems, the interactions among multiple degrees of freedom (spin, lattice, orbital, and charge) establish subtle balances among rich quantum states, which provide unique opportunities for abundant functionalities, including but not limited to high-temperature superconductivity, colossal magnetoresistivity, and multiferroicity [1–7].

In the past decade, the spin-orbit coupling (SOC) has attracted more and more attention in many branches of condensed matter. In particular, for those heavy transition metal elements with $4d$ or $5d$ orbitals, the synergetic effect of SOC and electron correlation can lead to emergent quantum phenomena such as topological phase [8–10], unconventional superconductivity [11–14], Kitaev spin liquid [15,16], large anisotropic magnetoresistivity [17,18], as well as magnetic quadrupole moments [19,20]. These SOC-entangled quantum states should be highly sensitive to external stimulations, which provides the opportunities to manipulate them. However, in such an emergent field, most attention has been focused on the realization of these quantum states and their unique physical properties, while the manipulation of these states is rarely touched upon until now.

Our recent theoretical work predicted that the $4d^1$ electron in K_2NbCl_6 is in the $J_{\text{eff}} = \frac{3}{2}$ state, which could be tuned to the $S = \frac{1}{2}$ state by rotating the spin axis [19]. A key characteristic of the ideal $J_{\text{eff}} = \frac{3}{2}$ state is that its spin magnetic moment and orbital magnetic moment should cancel each other, leading to a quenched net magnetic dipole moment

(i.e., ideally $0\mu_B/\text{Nb}$). However, a recent neutron study found that its sister compound Rb_2NbCl_6 exhibited a large magnetic moment up to $0.96\mu_B/\text{Nb}$ [20], which was close to the $S = \frac{1}{2}$ limit instead. For comparison, $A_2\text{TaCl}_6$ ($A = \text{K}, \text{Rb}, \text{Cs}$) with $5d^1$ electronic configuration exhibited much smaller magnetic moments $\sim 0.25\text{--}0.30\mu_B/\text{Ta}$ [20], closer to the $J_{\text{eff}} = \frac{3}{2}$ case, although not so ideal.

In this work, the underlying physics of these $J_{\text{eff}} = \frac{3}{2}$ candidates will be studied theoretically, to clarify why some of them are in the $S = \frac{1}{2}$ state while some are close to the $J_{\text{eff}} = \frac{3}{2}$ state. Besides the previously known SOC and Hubbard U , the tetragonal distortion (i.e., the static Jahn-Teller Q_3 mode) is found to play a decisive role in $J_{\text{eff}} = \frac{3}{2}$ states of $4d^1/5d^1$ systems. Furthermore, quantum phase transitions between the $S = \frac{1}{2}$ and $J_{\text{eff}} = \frac{3}{2}$ states, as well as between different $J_{\text{eff}} = \frac{3}{2}$ states, are tuned by epitaxial strain. Although the influences of Jahn-Teller distortion on physical properties have been touched more or less in these SOC systems [20–27], its essential role to the J_{eff} states, especially how to manipulate the J_{eff} states via the strain, has not been reported yet.

II. MODEL AND METHODS

The atomic SOC model Hamiltonian can be written as

$$H_{\text{SOC}} = \lambda \mathbf{L} \cdot \mathbf{S}, \quad (1)$$

where λ is the SOC coefficient, \mathbf{L} is the orbital moment operator, and \mathbf{S} is the spin operator.

In the octahedral crystal field, the d orbitals will be split into the low-lying t_{2g} triplets ($d_{xz}/d_{yz}/d_{xy}$) and higher-energy e_g doublets ($d_{3z^2-r^2}/d_{x^2-y^2}$). For electron configurations from d^1 to d^3 , the e_g doublets can be neglected, and only the t_{2g} triplets are essential. If the tetragonal distortion is considered, there will be an on-site energy splitting between d_{xz}/d_{yz} and d_{xy} . The details of the SOC model Hamiltonian for t_{2g} levels

*wyk@njupt.edu.cn

†sdong@seu.edu.cn

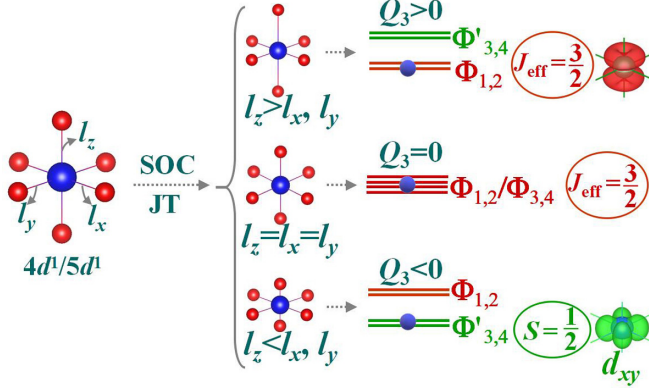


FIG. 1. Schematic of the collaborative effect of SOC and Q_3 mode distortion for the $4d^1/5d^1$ electron states in the octahedral crystal field. Here, Q_3 is defined as $(2l_z - l_x - l_y)/\sqrt{6}$, where l denotes the bond length along a particular axis [34]. For an undistorted octahedron (i.e., $Q_3 = 0$), the SOC leads to four degenerate low-lying $J_{\text{eff}} = \frac{3}{2}$ levels (Φ_1 , Φ_2 , Φ_3 , and Φ_4) and high-lying $J_{\text{eff}} = \frac{1}{2}$ doublets (not shown here). For the d^1 configuration, the $J_{\text{eff}} = \frac{3}{2}$ levels are quarter-filled. For nonzero Q_3 , the $J_{\text{eff}} = \frac{3}{2}$ levels are split into two groups: Φ_1/Φ_2 and Φ'_3/Φ'_4 , the latter of which are mixed with the $J_{\text{eff}} = \frac{1}{2}$ states, more or less. Once this mixture is heavy, Φ'_3/Φ'_4 are close to the $S = \frac{1}{2}$ states. The sign of Q_3 determines whether Φ_1 (Φ_2) or Φ'_3 (Φ'_4) is the lowest-energy one.

and its solution can be found in the Supplemental Material (SM) [28].

In addition to the model study, concrete materials are also studied by density functional theory (DFT). Our DFT calculations were performed using the projector augmented wave pseudopotentials as implemented in the Vienna *ab initio* Simulation Package (VASP) code [29,30]. The revised Perdew-Burke-Ernzerhof for solids functional and the generalized gradient approximation (GGA) method are adopted to describe the crystalline structure and electron correlation [31]. Using the Dudarev implementation [32], the Hubbard repulsion U_{eff} 's are imposed on Nb's $4d$ and Ta's $5d$ orbitals. The cutoff energy of the plane wave is 450 eV and the $7 \times 7 \times 5$ Monkhorst-Pack k -point mesh is centered at the Γ point. Both the lattice constants and atomic positions are fully relaxed until the Hellman-Feynman forces converged to less than 0.01 eV/Å.

III. RESULTS AND DISCUSSION

A. Atomic orbital model

To give an elegant physical scenario, let us start from a local atomic orbital model. The atomic SOC can split the t_{2g} levels into the low-lying $J_{\text{eff}} = \frac{3}{2}$ quartets and higher-energy $J_{\text{eff}} = \frac{1}{2}$ doublets, as shown in Fig. 1. The wave functions of these low-lying $J_{\text{eff}} = \frac{3}{2}$ states can be expressed using the t_{2g} bases (d_{xy} , d_{yz} , d_{xz}) as follows [28]:

$$\begin{aligned}\Phi_1 &= \frac{1}{\sqrt{2}}(|d_{yz} \uparrow\rangle + i|d_{xz} \uparrow\rangle), \\ \Phi_2 &= \frac{1}{\sqrt{2}}(|d_{yz} \downarrow\rangle - i|d_{xz} \downarrow\rangle),\end{aligned}$$

$$\Phi_3 = \frac{1}{\sqrt{6}}(|d_{yz} \downarrow\rangle + i|d_{xz} \downarrow\rangle - 2|d_{xy} \uparrow\rangle),$$

$$\Phi_4 = \frac{1}{\sqrt{6}}(|d_{yz} \uparrow\rangle - i|d_{xz} \uparrow\rangle + 2|d_{xy} \downarrow\rangle), \quad (2)$$

where \uparrow/\downarrow denote the spin up/down. And the wave functions of higher-energy $J_{\text{eff}} = \frac{1}{2}$ states can be expressed as

$$\Phi_5 = \frac{1}{\sqrt{3}}(|d_{yz} \downarrow\rangle + i|d_{xz} \downarrow\rangle + |d_{xy} \uparrow\rangle),$$

$$\Phi_6 = \frac{1}{\sqrt{3}}(|d_{yz} \uparrow\rangle - i|d_{xz} \uparrow\rangle - |d_{xy} \downarrow\rangle). \quad (3)$$

Then, for the d^1 configuration, the $J_{\text{eff}} = \frac{3}{2}$ levels are quarter-filled, as sketched in Fig. 1. The one electron can occupy any of the Φ_i 's ($i = 1-4$) or their linear combinations. The other three levels can be pushed upward in energy by the Hubbard repulsion, and a Mott gap can be opened if the Hubbard U is enough, resulting in a $J_{\text{eff}} = \frac{3}{2}$ Mott state. Such a scenario is a standard one to demonstrate the J_{eff} states, similar to the $J_{\text{eff}} = \frac{1}{2}$ case [33].

However, for such a system with partially occupied degenerate levels, the tetragonal distortion should be active. In fact, in all $A_2\text{NbCl}_6$ and $A_2\text{TaCl}_6$ (as well as Sr_2IrO_4), their octahedra are distorted, with different bond lengths along the z axis and in the x - y plane, as sketched in Fig. 1. Such a tetragonal distortion can lift the degeneracy between d_{xy} and d_{xz}/d_{yz} , characterized by the coefficient ω (the ratio of distortion energy splitting and the SOC coefficient, as explained in the SM [28]), which is in proportion to the intensity of the Q_3 mode distortion. Then the eigenenergies [Fig. 2(a)] and corresponding wave functions of the t_{2g} levels can be obtained.

Comparing with the undistorted case, Φ_1 and Φ_2 are not affected since they only involve d_{xz} and d_{yz} . However, Φ'_3 and Φ'_4 deviate from their ideal limits, by mixing some $J_{\text{eff}} = \frac{1}{2}$ components. In particular, Φ'_i ($i = 3-6$) can be expressed as

$$\begin{aligned}\Phi'_3 &= \frac{1}{\sqrt{2+a^2}}(|d_{yz} \downarrow\rangle + i|d_{xz} \downarrow\rangle + a|d_{xy} \uparrow\rangle), \\ \Phi'_4 &= \frac{1}{\sqrt{2+a^2}}(|d_{yz} \uparrow\rangle - i|d_{xz} \uparrow\rangle - a|d_{xy} \downarrow\rangle), \\ \Phi'_5 &= \frac{1}{\sqrt{2+b^2}}(|d_{yz} \downarrow\rangle + i|d_{xz} \downarrow\rangle + b|d_{xy} \uparrow\rangle), \\ \Phi'_6 &= \frac{1}{\sqrt{2+b^2}}(|d_{yz} \uparrow\rangle - i|d_{xz} \uparrow\rangle - b|d_{xy} \downarrow\rangle),\end{aligned} \quad (4)$$

where $a = [(\omega - 1) - \sqrt{(\omega - 1)^2 + 8}]/2$ and $b = [(\omega - 1) + \sqrt{(\omega - 1)^2 + 8}]/2$. Then the evolution of the d_{xy} , d_{yz} , and d_{xz} weights in Φ'_i ($i = 3-6$) can be obtained as a function of ω , as shown in Fig. 2(b).

In particular, for the tetragonal elongation ($Q_3 > 0$, i.e., $\omega > 0$), Φ_1 and Φ_2 are lower in energy than Φ'_3 and Φ'_4 , since the on-site energy of d_{xy} is higher than that of d_{xz}/d_{yz} . Thus, the ground state remains the ideal $J_{\text{eff}} = \frac{3}{2}$ state. In contrast, for the tetragonal compression ($Q_3 < 0$), the lower-energy d_{xy} orbital makes Φ'_3 and Φ'_4 more favorable. For the ideal Φ_3 or Φ_4 , the weight of the d_{xy} orbital already reaches 66.7%. The negative Q_3 (ω) will further enhance its weight. In the

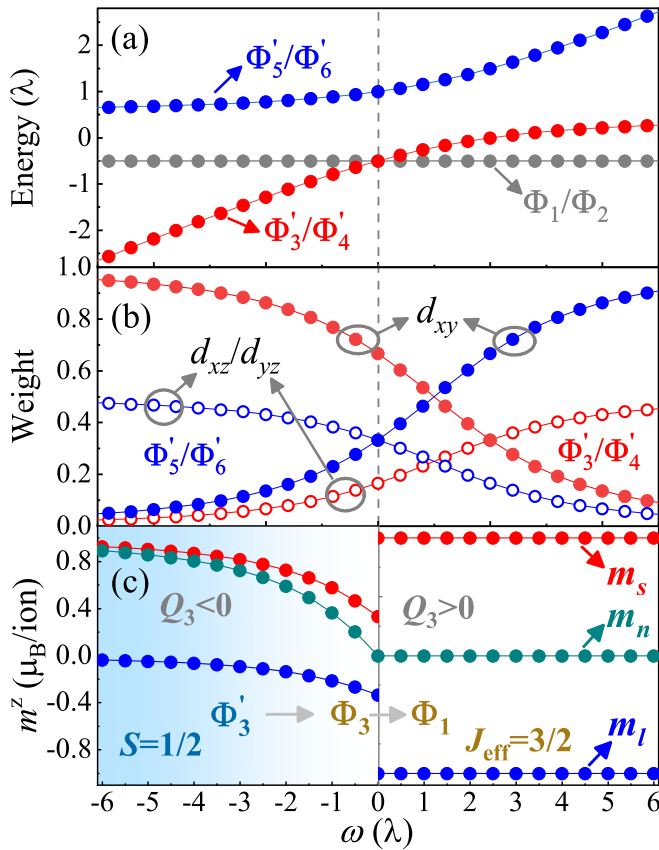


FIG. 2. Numerical results of the atomic orbital model to demonstrate the scenario proposed in Fig. 1. (a) Eigenenergies, (b) t_{2g} orbital weights, and (c) spin (m_s) and orbital (m_l) magnetic moments (along the z axis), as a function of Q_3 intensity, characterized by ω . The ω and eigenenergy are in units of λ , the SOC coefficient. In (b), the red and blue symbols are for Φ'_3 (Φ'_4) and Φ'_5 (Φ'_6), respectively. m_n : net magnetic moment ($= m_l + m_s$).

large limit of negative Q_3 , Φ'_3 or Φ'_4 will be eventually close to the pure d_{xy} orbital, i.e., an $S = \frac{1}{2}$ state. In this sense, the tetragonal distortion can tune the phase transitions between the $J_{\text{eff}} = \frac{3}{2}$ states and the $S = \frac{1}{2}$ one.

The ω -dependent magnetic moments of Φ_1 (or Φ_2) and Φ'_3 (or Φ'_4) are presented in Fig. 2(c), including both the spin component and orbital component. For the positive Q_3 case ($\omega > 0$), the occupied state is always Φ_1 or Φ_2 , which will be split by Hubbard repulsion. The most interesting physical property of Φ_1 (or Φ_2) is that its spin magnetic moment ($1\mu_B$) just cancels the orbital magnetic moment ($-1\mu_B$), leading to a zero net magnetization [19]. In the opposite direction, i.e., $\omega < 0$, Φ'_3 (or Φ'_4) becomes the low-lying level. With increasing negative ω , Φ'_3 's spin magnetic moment along the z axis gradually increases from $\frac{1}{3}\mu_B$ to approach the limit $1\mu_B$, while the orbital magnetic moment gradually decreases from $-\frac{1}{3}\mu_B$ to the limit $0\mu_B$, as expected for the transition from the $J_{\text{eff}} = \frac{3}{2}$ state to the $S = \frac{1}{2}$ state.

B. Materials

The aforementioned physical scenario can be well demonstrated in real materials, e.g., hexachlorides A_2MCl_6 ($A = \text{K},$

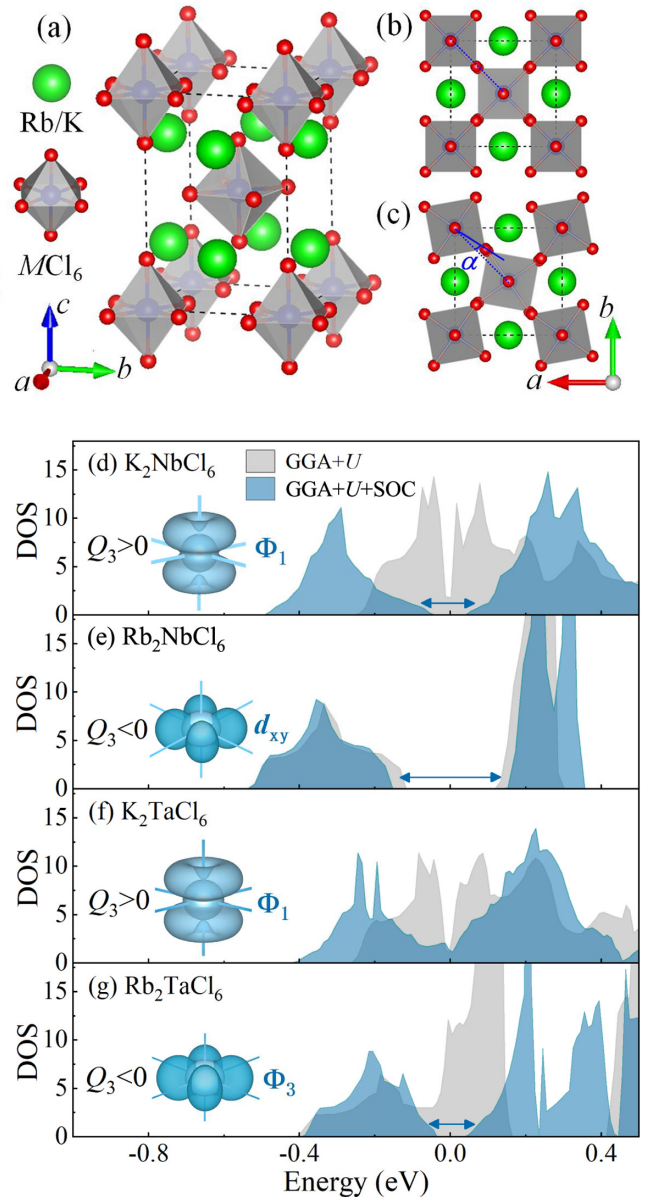


FIG. 3. (a)–(c) Schematic crystal structures of A_2MCl_6 . (b) Top view of $A = \text{Rb}$, space group $I4/mmm$ (No. 139). (c) Top view of $A = \text{K}$, space group $P4/mnc$ (No. 128). The smaller K ion leads to a smaller in-plane lattice constant, which results in the elongation (i.e., $Q_3 > 0$) and rotation of octahedra. Since these octahedra are almost isolated, the effect of octahedral rotation to the electronic states is negligible. (d)–(g) Comparison of density of states (DOS) between the GGA+ U and GGA+ U +SOC calculations. Here, $U_{\text{eff}} = 1$ and 0.7 eV are applied on Nb's $4d$ and Ta's $5d$ orbitals, respectively. Insets: the electron clouds of valence bands near the Fermi level, i.e., the d^1 electrons.

$\text{Rb}, \text{Cs}; M = \text{Nb}, \text{Ta}$). The crystal structures of this family are shown in Figs. 3(a)–3(c). Unlike perovskite oxides where oxygen octahedra are connected via the corner-, edge-, or face-sharing manner, these MCl_6 octahedra are nearly isolated [26]. In this sense, the electron hoppings between M ions are significantly suppressed, leading to narrow bands near the Fermi level. According to their experimental structures [20,26], all MCl_6 octahedra in these hexachlorides are tetrag-

TABLE I. DFT calculated magnetic moments of A_2MCl_6 in units of μ_B/M , including the spin magnetic moments (m_s), orbital magnetic moments (m_l), and the net moments ($m_n = m_s + m_l$).

	K_2NbCl_6	Rb_2NbCl_6	K_2TaCl_6	Rb_2TaCl_6
m_s	0.877	0.733	0.694	0.343
m_l	-0.697	-0.100	-0.522	-0.316
m_n	0.180	0.633	0.172	0.027
State	Φ_1	d_{xy}	Φ_1	Φ_3

onally distorted, i.e., with the static Jahn-Teller Q_3 mode distortion. In addition, the d - p hybridization in the chloride family is much weaker than that in oxides, which makes the d -orbital levels more pure. In this sense, these MCl_6 octahedra provide an ideal playground to study the SOC-assisted Mottness of its $4d/5d$ orbitals.

Previously, some of the hexachlorides A_2MCl_6 (e.g., A_2TaCl_6 , K_2NbCl_6) were claimed to host the $J_{\text{eff}} = \frac{3}{2}$ state [19,20], while Rb_2NbCl_6 was found to be close to the $S = \frac{1}{2}$ state [20]. These puzzling contradictions can be well answered in our DFT calculations [28], as summarized in Figs. 3(d)–3(g), Table I, as well as Table S1 in the SM [28].

In K_2NbCl_6 , the $NbCl_6$ octahedra are spontaneously elongated along the crystalline c axis (i.e., the z axis of octahedra), i.e., $Q_3 > 0$, which prefers the pure $J_{\text{eff}} = \frac{3}{2}$ state Φ_1 (or Φ_2) [Fig. 3(d)]. The spin and orbital magnetic moments obtained in our DFT calculation are close to their ideal limits (see Table I). The band gap can only be opened with the help of SOC, implying the SOC-assisted Mottness [19].

In contrast, for Rb_2NbCl_6 , the $NbCl_6$ octahedra are spontaneously compressed along the crystalline c axis (i.e., the z axis of octahedra), i.e., $Q_3 < 0$, which prefers the Φ'_3 (or Φ'_4) state [Fig. 3(e)]. And a band gap is already opened even without SOC, due to the tetragonal distortion splitting. Meanwhile, its spin magnetic moment is large but its orbital magnetic moment is rather small (see Table I), in agreement with the experimental large magnetic moment [20]. Therefore, this distorted Φ'_3 (or Φ'_4) is closer to $S = \frac{1}{2}$ (d_{xy}), instead of the $J_{\text{eff}} = \frac{3}{2}$ state Φ_3 (or Φ_4). Previously, the absence of the $J_{\text{eff}} = \frac{3}{2}$ state in Rb_2NbCl_6 was attributed to its relative weak SOC intensity of $4d$ orbitals [20]. However, the present work suggests a more decisive role of Q_3 mode distortion in Rb_2NbCl_6 ; since its sister member K_2NbCl_6 can exhibit the pure $J_{\text{eff}} = \frac{3}{2}$ state [19], even its SOC intensity is not as strong as the $5d$ counterparts.

The story of K_2TaCl_6 is very similar to K_2NbCl_6 , with a positive Q_3 and an even larger SOC, which can lead to the Φ_1 (or Φ_2) state, as shown in Fig. 3(f). The only difference is that the weaker Hubbard U of $5d$ orbitals may be not insufficient to open a Mott gap.

The story of Rb_2TaCl_6 is unique. Its Q_3 mode is negative, which seems to be similar to Rb_2NbCl_6 . However, the large SOC of $5d$ orbitals makes a small ω (the ratio between tetragonal distortion splitting and the SOC coefficient). Thus the $5d^1$ state in Rb_2TaCl_6 is close to $J_{\text{eff}} = \frac{3}{2}$ (Φ_3 or Φ_4), instead of $S = \frac{1}{2}$ (d_{xy}). As evidence of Φ_3 , its spin and orbital magnetic moments are close to $\frac{1}{3}$ and $-\frac{1}{3}\mu_B/Nb$, respectively (see Table I).

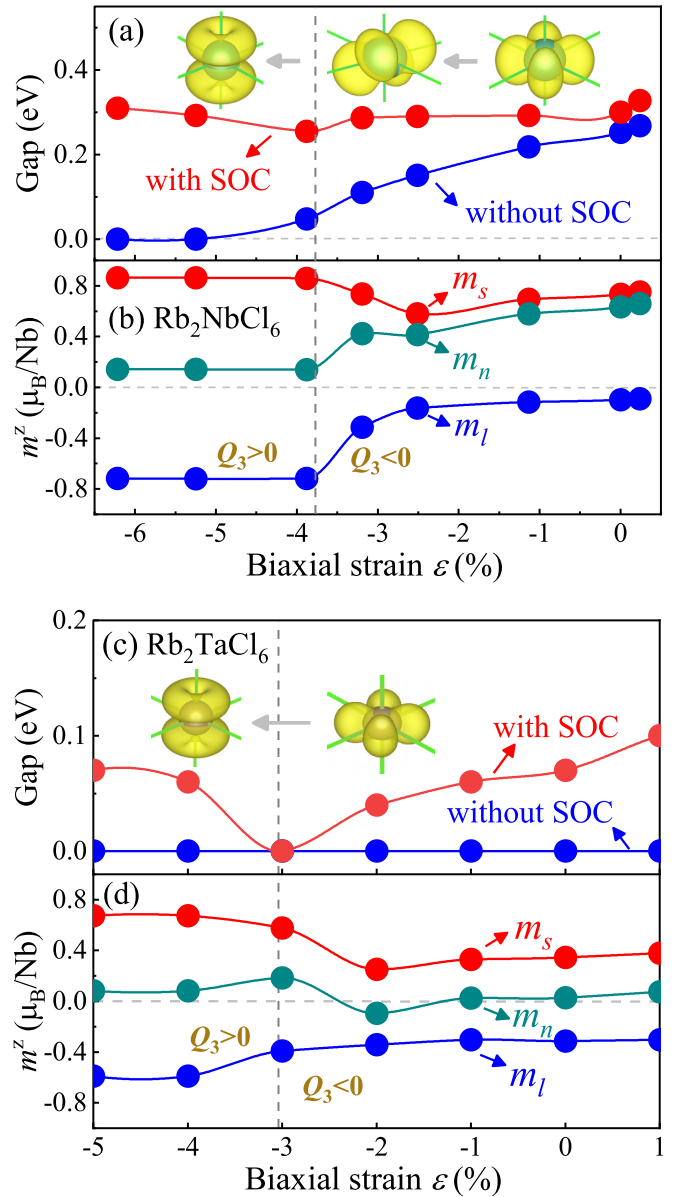


FIG. 4. Biaxial strain tuned electronic state transitions between $S = \frac{1}{2}$ and $J_{\text{eff}} = \frac{3}{2}$ (Φ_1 and Φ_3) in (a), (b) Rb_2NbCl_6 and (c), (d) Rb_2TaCl_6 . (a) and (c) The band gaps (with/without SOC). (b) and (d) The magnetic moments of a Nb/Ta ion (with SOC). The boundary $Q_3 = 0$ (vertical broken line) locates at $\varepsilon \sim -3.8\%$ and $\varepsilon \sim -3.0\%$, respectively. Insets: the electron clouds of valence bands near the Fermi levels.

C. Strain tuning of $J_{\text{eff}} = \frac{3}{2}$ states

Although the $4d^1$ electron in Rb_2NbCl_6 is not in the $J_{\text{eff}} = \frac{3}{2}$ state, it provides an appropriate candidate to study the strain effect. Here the epitaxial biaxial strain is imposed to control the sign and amplitude of the Q_3 mode. The biaxial strain is defined as $\varepsilon = (a - a_0)/a_0$, where a_0 and a are the in-plane lattice constants before and after the strain, respectively. Upon the biaxial strain, the atomic positions and lattice constant along the c axis are further optimized.

As shown in Fig. 4(a), without SOC, the band gap is gradually closed with increasing compressive strain. This is due to the half-filling of the low-lying degenerate d_{yz} and d_{xz} orbitals

in the positive Q_3 case. However, the SOC can open the band gap by forming the J_{eff} state (Φ_1 or Φ_2). In other words, the band gap ~ 0.3 eV in the whole presented region of ε is driven by different mechanisms: (1) Q_3+U in the $S = \frac{1}{2}$ side; (2) SOC+ U in the $J_{\text{eff}} = \frac{3}{2}$ side.

Correspondingly, the evolution of magnetic moments is shown in Fig. 4(b). When Q_3 turns to be positive, the spin moment slightly increases from $\sim 0.7\mu_B/\text{Nb}$ to $\sim 0.9\mu_B/\text{Nb}$, while the orbital moment increases rapidly from $\sim -0.1\mu_B/\text{Nb}$ to $\sim -0.7\mu_B/\text{Nb}$, indicating the transition from the $S = \frac{1}{2}$ state to the $J_{\text{eff}} = \frac{3}{2}$ one.

For comparison, the strain effect to Rb_2TaCl_6 is also studied, which provides an appropriate candidate to tune the two states of $J_{\text{eff}} = \frac{3}{2}$ (Φ_1 vs Φ_3). As shown in Fig. 4(c), without SOC, the system is always metallic in the whole strain range, due to the weaker Hubbard repulsion ($U_{\text{eff}} = 0.7$ eV used here) and more spatially expanding wave function of $5d$ orbitals. With increasing compressive strain, the band gap (opened by SOC) gradually decreases to zero and reopens. The gap closing point is just at the $Q_3 = 0$ boundary, at which Φ_i 's ($i = 1-4$) are originally degenerated (before the Hubbard splitting). This $Q_3 = 0$ boundary just separates Φ_1 and Φ_3 , although both of them are $J_{\text{eff}} = \frac{3}{2}$ states.

This transition can be also evidenced in the magnetic moments, as shown in Fig. 4(d). Although the net magnetic moment is always close to zero in the whole range, the spin magnetic moment and orbital magnetic moment change from $\sim 0.3\mu_B/\text{Ta}$ to $\sim 0.7\mu_B/\text{Ta}$.

All the above results demonstrated that the J_{eff} states in the $4d^1$ and $5d^1$ systems could be efficiently tuned by strain, via the tetragonal distortion.

IV. SUMMARY

Our theoretical studies, based on both the atomic orbital model and first-principles calculations, clarified the divergent results regarding the $J_{\text{eff}} = \frac{3}{2}$ states in the $4d^1$ and $5d^1$ systems. Different from the previous argument which relied on the difference of SOC intensity [37], our study highlighted the key role of the Q_3 mode distortion. With different signs of Q_3 mode and SOC intensities, four typical hexachlorides, K_2NbCl_6 , Rb_2NbCl_6 , K_2TaCl_6 , and Rb_2TaCl_6 , own three types of electronic states: $J_{\text{eff}} = \frac{3}{2}$ state Φ_1 (or Φ_2) for both K_2NbCl_6 and K_2TaCl_6 ; $J_{\text{eff}} = \frac{3}{2}$ state Φ_3 (or Φ_4) for Rb_2TaCl_6 ; but $S = \frac{1}{2}$ state d_{xy} for Rb_2NbCl_6 . In addition, our work also proposed an efficient route to control these electronic states in $4d^1/5d^1$ systems. By tuning the tetragonal distortion through epitaxial strain, quantum phase transitions between these three states can be achieved. Following experiments are encouraged to manipulate these $J_{\text{eff}} = \frac{3}{2}$ quantum states in this way. More theoretical investigations on other distortions beyond the simplest Q_3 mode are also encouraged, which may lead to more emergent physical phenomena in these strong SOC quantum materials.

ACKNOWLEDGMENTS

This work was supported by the National Natural Science Foundation of China (Grants No. 11804168 and No. 11834002), the Natural Science Foundation of Jiangsu Province (Grant No. BK20180736), and NUPTSF (Grant No. NY219026).

-
- [1] M. Imada, A. Fujimori, and Y. Tokura, *Rev. Mod. Phys.* **70**, 1039 (1998).
 - [2] E. Dagotto, *Science* **309**, 257 (2005).
 - [3] E. Dagotto and Y. Tokura, *MRS Bull.* **33**, 1037 (2008).
 - [4] J. Chakhalian, J. W. Freeland, A. J. Millis, C. Panagopoulos, and J. M. Rondinelli, *Rev. Mod. Phys.* **86**, 1189 (2014).
 - [5] P. Zubko, S. Gariglio, M. Gabay, P. Ghosez, and J.-M. Triscone, *Annu. Rev. Condens. Matter Phys.* **2**, 141 (2011).
 - [6] S. Dong, J.-M. Liu, S.-W. Cheong, and Z. F. Ren, *Adv. Phys.* **64**, 519 (2015).
 - [7] S. Dong, H. J. Xiang, and E. Dagotto, *Natl. Sci. Rev.* **6**, 629 (2019).
 - [8] D. Pesin and L. Balents, *Nat. Phys.* **6**, 376 (2010).
 - [9] X. Wan, A. M. Turner, A. Vishwanath, and S. Y. Savrasov, *Phys. Rev. B* **83**, 205101 (2011).
 - [10] W. Witczak-Krempa and Y. B. Kim, *Phys. Rev. B* **85**, 045124 (2012).
 - [11] F. Wang and T. Senthil, *Phys. Rev. Lett.* **106**, 136402 (2011).
 - [12] H. Watanabe, T. Shirakawa, and S. Yunoki, *Phys. Rev. Lett.* **110**, 027002 (2013).
 - [13] Y. J. Yan, M. Q. Ren, H. C. Xu, B. P. Xie, R. Tao, H. Y. Choi, N. Lee, Y. J. Choi, T. Zhang, and D. L. Feng, *Phys. Rev. X* **5**, 041018 (2015).
 - [14] Y. K. Kim, N. H. Sung, J. D. Denlinger, and B. J. Kim, *Nat. Phys.* **12**, 37 (2016).
 - [15] G. Jackeli and G. Khaliullin, *Phys. Rev. Lett.* **102**, 017205 (2009).
 - [16] H. Takagi, T. Takayama, G. Jackeli, G. Khaliullin, and S. E. Nagler, *Nat. Rev. Phys.* **1**, 264 (2019).
 - [17] C. L. Lu, B. Gao, H. W. Wang, W. Wang, S. L. Yuan, S. Dong, and J.-M. Liu, *Adv. Funct. Mater.* **28**, 1706589 (2018).
 - [18] H. W. Wang, C. L. Lu, J. Chen, Y. Liu, S. L. Yuan, S.-W. Cheong, S. Dong, and J.-M. Liu, *Nat. Commun.* **10**, 2280 (2019).
 - [19] Y. K. Weng, X. Li, and S. Dong, *Phys. Rev. B* **102**, 180401(R) (2020).
 - [20] H. Ishikawa, T. Takayama, R. K. Kremer, J. Nuss, R. Dinnebier, K. Kitagawa, K. Ishii, and H. Takagi, *Phys. Rev. B* **100**, 045142 (2019).
 - [21] L. Xu, N. A. Bogdanov, A. Princep, P. Fulde, J. van den Brink, and L. Hozoi, *npj Quantum Mater.* **1**, 16029 (2016).
 - [22] N. Iwahara, V. Vieru, and L. F. Chibotaru, *Phys. Rev. B* **98**, 075138 (2018).
 - [23] D. Fiore Mosca, L. V. Pourovskii, B. H. Kim, P. Liu, S. Sanna, F. Boscherini, S. Khmelevskiy, and C. Franchini, *Phys. Rev. B* **103**, 104401 (2021).
 - [24] H. Liu and G. Khaliullin, *Phys. Rev. Lett.* **122**, 057203 (2019).

- [25] E. M. Plotnikova, M. Daghofer, J. van den Brink, and K. Wohlfeld, *Phys. Rev. Lett.* **116**, 106401 (2016).
- [26] H. Henke, *Z. Kristallogr.* **222**, 477 (2007).
- [27] S. V. Streltsov and D. I. Khomskii, *Phys. Rev. X* **10**, 031043 (2020).
- [28] See Supplemental Material at <http://link.aps.org/supplemental/10.1103/PhysRevB.104.165150>, which includes analytic derivations of distorted $J_{\text{eff}} = \frac{3}{2}$ states and more DFT results, as well as Refs. [19,20,26,29–32,35,36].
- [29] P. E. Blöchl, *Phys. Rev. B* **50**, 17953 (1994).
- [30] G. Kresse and D. Joubert, *Phys. Rev. B* **59**, 1758 (1999).
- [31] J. P. Perdew, A. Ruzsinszky, G. I. Csonka, O. A. Vydrov, G. E. Scuseria, L. A. Constantin, X. Zhou, and K. Burke, *Phys. Rev. Lett.* **100**, 136406 (2008).
- [32] S. L. Dudarev, G. A. Botton, S. Y. Savrasov, C. J. Humphreys, and A. P. Sutton, *Phys. Rev. B* **57**, 1505 (1998).
- [33] B. J. Kim, H. Jin, S. J. Moon, J.-Y. Kim, B.-G. Park, C. S. Leem, J. Yu, T. W. Noh, C. Kim, S.-J. Oh, J.-H. Park, V. Durairaj, G. Cao, and E. Rotenberg, *Phys. Rev. Lett.* **101**, 076402 (2008).
- [34] S. Dong, X. T. Zhang, R. Yu, J.-M. Liu, and E. Dagotto, *Phys. Rev. B* **84**, 155117 (2011).
- [35] J. G. He and C. Franchini, *Phys. Rev. B* **86**, 235117 (2012).
- [36] M. An, Y. K. Weng, H. M. Zhang, J.-J. Zhang, Y. Zhang, and S. Dong, *Phys. Rev. B* **96**, 235112 (2017).
- [37] G. Chen, R. Pereira, and L. Balents, *Phys. Rev. B* **82**, 174440 (2010).